AIMS Mathematics, 9(12): 35978–36000.
DOI: 10.3934/math.20241706
Received: 22 September 2024
Revised: 19 November 2024
Accepted: 13 December 2024
Published: 25 December 2024

https://www.aimspress.com/journal/Math

Research article

Applications of mixed finite element method based on Bernstein polynomials in numerical solution of Stokes equations

Lanyin Sun* **and Siya Wen**

School of Mathematics and Statistics, Xinyang Normal University, Xinyang, 464000, China

* **Correspondence:** Email: lysun@xynu.edu.cn.

Abstract: The Stokes equation is fundamental in fluid mechanics. We used bivariate Bernstein polynomial bases to construct the function space for mixed finite element methods to solve the 2D Stokes equation. Our results show that the numerical accuracy and convergence order using bicubic and lower-order Lagrange interpolation polynomials are comparable to those achieved with Bernstein polynomial bases. However, high-order Lagrange interpolation functions often suffer from the Runge's phenomenon, which limits their effectiveness. By employing high-order Bernstein polynomial bases, we have significantly improved the numerical solutions, effectively mitigating the Runge phenomenon. This approach highlights the advantages of Bernstein polynomial bases in achieving stable and accurate solutions for the 2D Stokes equation.

Keywords: mixed finite element method; Bernstein polynomial basis; 2D Stokes equations
Mathematics Subject Classification: 65D17, 65M60

1. Introduction

The Stokes equation [1] is a fundamental tool used to describe viscous fluid flow [2] at low Reynolds numbers (Re) [3], which typically indicates laminar flow conditions [4]. Re characterizes the ratio of inertial forces to viscous forces in fluid dynamics. When Re is very small, the characteristic velocity of the flow can be considered to approach zero. In this limit, the quadratic terms involving velocity in the Navier-Stokes equations become negligible. Consequently, the Navier-Stokes equations simplify the Stokes equations, helping to analyze more complicated fluid problems, with a very wide range of applications [5, 6]. With the development of computer science, many numerical methods have been developed to solve Stokes problems, such as finite element method (FEM) [7–9], finite difference method [10], mixed FEM [11], boundary element method [12, 13], and coupling of FEM [14]. Among them, the FEM has gradually become an important numerical computational method for approximating partial differential equations (PDEs) because of its many advantages such as strong program versatility,

high accuracy, flexible mesh selection, and ability to deal with complex boundaries and high-order problems.

The FEM, as an important numerical method for solving mathematical [15] and physical problems [16], has been widely applied in the field of engineering mechanics [17]. In 1943, Courant [18] introduced the concept of FEM by using continuous functions on triangular regions to solve the torsion problem of St. Venant. By the mid-1960s, Feng [19,20] had independently established the mathematical foundation of FEM, making it a systematic and widely used numerical method. Since then, the scope of FEM's application has expanded from single structural analysis to various fields such as sound field analysis, flow field analysis, and electromagnetic field analysis. Based on the variational principle and subdivision interpolation, FEM uses interpolation functions in each element to approximate the unknown function in the domain piece by piece.

With the continuous progress of computer science, the FEM has undergone remarkable developments and improvements. Many new computational methods have emerged, including the finite volume method [21], upwind FEM [22], and spectral methods [23]. These new methods not only enrich the technical means of numerical simulation but also play a crucial role in improving computational efficiency and enhancing model accuracy. In the FEM, the selection of finite element basis functions is key, and appropriate test and trial function spaces ensure the accuracy and stability of the solution. Common choices include Lagrange functions [24], Hermite functions [25], Argyris functions [26], and Bernstein functions [27]. In 1979, Shi [28] used cubic B-spline variational methods to solve equilibrium problems in composite elastic structures of plates and beams in regular domains, introducing spline FEM. In the same year, Qin [29] proposed the spline finite point method based on spline functions, beam vibration functions, and energy variation. In 2005, Hughes et al. [30] used spline basis functions for approximate numerical calculations of field variables in physical problems in finite element analysis. In 2007, Bhatti and Bracken [27] proposed applying Bernstein polynomial bases to solve PDEs. Zhu and Kang [31], in 2010, used cubic B-spline quasi-interpolation to numerically solve the Burgers-Fisher equation. Dutykh [32], in 2014, solved the KdV and KdV-BBM equations using B-spline FEM. More recently in 2022, Pranta [33] solved 2D nonlinear parabolic PDEs using bicubic Bernstein polynomial bases. These developments highlight the ongoing evolution and versatility of FEM in addressing complex engineering and scientific challenges.

Lagrange interpolation functions are typically global, offering high accuracy in certain scenarios but potentially leading to numerical instability, especially with high-degree polynomials or complex boundary conditions. Although the Runge phenomenon [34] is less pronounced in FEM due to the integral approximation approach, it can still occur in specific cases, particularly with high-order polynomials or complex boundaries. Conversely, Bernstein polynomial functions have local support, enhancing numerical stability. They facilitate the construction of higher-order test and trial function spaces and are adept at handling complex boundary conditions. Additionally, Bernstein polynomials are non-negative and shape-preserving, making them uniquely suitable for shape-preserving approximations. Therefore, we have chosen Bernstein polynomial basis functions for our FEM implementation to ensure enhanced numerical stability and accuracy. However, it is important to note that Bernstein polynomials also have some limitations. While they offer stability and flexibility, the computational cost can increase significantly with higher polynomial degrees, making them less efficient for large-scale or real-time applications. Moreover, the theoretical foundation for certain specific problems, such as those involving very-high-order polynomials or highly oscillatory functions,

may still require further research and development.

Consider the boundary value problem of the 2D Stokes equation,

$$\begin{cases} -\nabla \cdot \mathbb{T}(\mathbf{u}, p) = \mathbf{f}, & in \quad \Omega, \\ \nabla \cdot \mathbf{u} = 0, & a.e. \quad in \ \Omega, \\ \mathbf{u} = \mathbf{g}, & a.e. \quad in \ \partial\Omega, \end{cases} \tag{1.1}$$

where $\Omega \subset \mathbb{R}^2$ is a bounded polygonal domain, $\mathbf{u} = \mathbf{u}(x, y)$ is the velocity vector, p refers to fluid pressure, $\nabla \cdot \mathbf{u}$ is the divergence of $\mathbf{u}$, and $\mathbb{T}(\mathbf{u}, p) = 2\nu\mathbb{D}(u) - p\mathbb{I}$ is the stress tensor. In more details, the deformation tensor can be written as

$$\mathbb{D}(\mathbf{u}) = \begin{pmatrix} \frac{\partial u_1}{\partial x} & \frac{1}{2}\left(\frac{\partial u_1}{\partial y} + \frac{\partial u_2}{\partial x}\right) \\ \frac{1}{2}\left(\frac{\partial u_1}{\partial y} + \frac{\partial u_2}{\partial x}\right) & \frac{\partial u_2}{\partial y} \end{pmatrix}. \tag{1.2}$$

Hence, the stress tensor can be written as

$$\mathbb{T}(\mathbf{u}, p) = \begin{pmatrix} 2\nu\frac{\partial u_1}{\partial x} - p & \nu\left(\frac{\partial u_1}{\partial y} + \frac{\partial u_2}{\partial x}\right) \\ \nu\left(\frac{\partial u_1}{\partial y} + \frac{\partial u_2}{\partial x}\right) & 2\nu\frac{\partial u_2}{\partial y} - p \end{pmatrix}. \tag{1.3}$$

$\mathbf{f}$ describes the external force, $\mathbf{g}$ is the velocity on the domain boundary, and $\nu = \frac{UL}{Re}$ represents the kinematic viscosity of the fluid where U and L represent characteristic speed and characteristic length, respectively. The Stokes equation is a basic equation of fluid mechanics, which simulates the motion of low velocity or viscous fluid [35, 36] and has important applications in fluid mechanics [37], geophysics [38], telecommunication technology [39], and aerospace [40], among others [41–43]. We use the mixed FEM based on Bernstein polynomial basis to solve Stokes equations, and calculate the errors of the L^∞, L^2, and H^1-semi norms.

The traditional FEM is a versatile numerical technique that can handle both univariate and multivariate equations. However, when applied to systems involving multiple physical quantities, such as the Stokes equation (Eq (1.1)), traditional FEM requires careful consideration to ensure the existence and uniqueness of the solution. The Stokes equation involves a tight coupling between velocity and pressure, which necessitates precise numerical treatment. To guarantee the uniqueness [44] of the solution to the variational problem, the finite element approximation space must satisfy the Lax-Milgram theorem [45]. Additionally, to ensure the stability of the solution, especially for coupled variables, the inf-sup condition [45] must be satisfied. While traditional FEM can theoretically meet these requirements, the selection of appropriate finite element spaces for velocity and pressure is crucial. If the selection is not appropriate, the solution can become unstable and lose accuracy. Therefore, to ensure that the finite element approximation for the Stokes equation is both convergent and stable, we have chosen the mixed FEM. The mixed FEM can better handle the coupling between velocity and pressure by selecting suitable finite element spaces for these variables. This approach more effectively satisfies the inf-sup condition, thereby providing a more stable and accurate solution. Besides, we found that only the gradient term of pressure appeared in the Stokes equation, which cannot guarantee that the solution of pressure is unique. Therefore, in the process of solving, we need to impose additional conditions for pressure. In this article, we fix pressure at one point in the region. Furthermore, the mixed FEM is not limited to the Stokes equation. It can be equally effective in other

multivariate systems, such as the velocity-stress formulation of the wave equation [46, 47]. By using mixed FEM, we can achieve higher accuracy and stability in solving a wide range of coupled PDEs.

This paper is organized as follows. In Section 2, we first review some basic contents of Bernstein polynomial basis, Bézier curves, and surfaces. In Section 3, we use the mixed FEM based on the Bernstein polynomial basis to derive the discrete scheme of Stokes equation. In Section 4, the error result is obtained by some numerical examples. In Section 5, we summarize the work.

2. Bernstein basis functions, curves, and surfaces

In this section, we will recall the definitions and properties of Bernstein polynomial bases, Bézier curves, and surfaces.

Definition 1. *Bernstein polynomial bases of degree n are defined by*

$$B_i^n(x) = \binom{n}{i} x^i (1-x)^{n-i}, i = 1, 2, \cdots, n, \tag{2.1}$$

where, $\binom{n}{i} = \frac{n!}{i!(n-i)!}, i = 0, 1, \cdots, n$. *For simplicity, when i<0 or i>n, let* $B_i^n(x) = 0, x \in [0, 1]$.

Definition 2. *Given control points* $P_i(x, y) \in \mathbb{R}^2 (i = 0, 1, \cdots, n)$, *the Bézier curve of n degrees is defined by*

$$P(x) = \sum_{i=0}^{n} P_i B_i^n(x), x \in [0, 1],$$

where $B_i^n(x)(i = 0, 1, \cdots, n)$ *is defined as Eq* (2.1)*, and the n-edge polygon obtained by connecting two adjacent control points with straight line segments is called the control polygon.*

Bernstein polynomial bases of tensor product type can be obtained by tensor product from Bernstein polynomial bases of one variable.

Definition 3. *The tensor product type Bernstein polynomial bases of* $m \times n$ *degree are defined by*

$$B_{i,j}^{m,n}(s, \tau) = B_i^m(s) B_j^n(\tau), i = 0, 1, \cdots, m, j = 0, 1, \cdots, n. \tag{2.2}$$

Definition 4. *For a continuous function* $f(s, \tau)$ *defined on* $[0, 1] \times [0, 1]$, *the tensor product Bernstein polynomial interpolation operator* B_h *is defined as*

$$B_h(f, s, \tau) = \sum_{i=0}^{m} \sum_{j=0}^{n} f B_{i,j}^{m,n}(s, \tau). \tag{2.3}$$

Next, we prove that B_h is a bounded interpolation operator.

Since f is a continuous function, it is bounded on $[0, 1] \times [0, 1]$. Therefore, there exists a constant

M such that $|f(s,\tau)| \le M$ for all $(s,\tau) \in [0,1] \times [0,1]$. Hence

$$\begin{aligned} |B_h(f,s,\tau)| &= |\sum_{i=0}^{m}\sum_{j=0}^{n} f B_{i,j}^{m,n}(s,\tau)| \\ &\le \sum_{i=0}^{m}\sum_{j=0}^{n} |f| B_{i,j}^{m,n}(s,\tau) \\ &\le M \sum_{i=0}^{m}\sum_{j=0}^{n} B_{i,j}^{m,n}(s,\tau) = M. \end{aligned} \tag{2.4}$$

So we can get that B_h is a bounded interpolation operator.

Since B_h is a bounded interpolation operator, by the Bramble-Hilbert Lemma [45], we can conclude that

$$\|\mathbf{u} - B_h(\mathbf{u})\|_{W^{k,p}} \le Ch^{L-k}\|\mathbf{u}\|_{W^{L,p}}, \quad k = 0, 1, \cdots, L.$$

3. Mixed finite element algorithm based on Bernstein polynomial basis for Stokes equations

In this section, we first construct function spaces of the mixed FEM with Bernstein polynomial basis, and the discrete scheme of Stokes equation in Eq (1.1) is derived.

3.1. Galerkin formulation

First of all, consider the subspace $H_0^1(\Omega)$ of Sobolev space $H^1(\Omega)$:

$$H_0^1(\Omega) = \left\{ u \in H^1(\Omega); u|_{\partial\Omega} = 0 \right\}.$$

Multiplying the first equation of Eq (1.1) by test vector function $\mathbf{v}(x,y) \in H_0^1(\Omega) \times H_0^1(\Omega)$ and then integrating on Ω yields

$$\int_\Omega (-\nabla \cdot \mathbb{T}(\mathbf{u}, p)) \cdot \mathbf{v}\, dxdy = \int_\Omega f \cdot \mathbf{v}\, dxdy.$$

Second, by multiplying the divergence-free equation by a test function $q(x,y)$, we get

$$\int_\Omega (\nabla \cdot \mathbf{u}) q\, dxdy = 0.$$

Then, applying Green's identity,

$$\begin{aligned} \int_\Omega 2\nu \mathbb{D}(\mathbf{u}) : \mathbb{D}(\mathbf{v})\, dxdy - \int_\Omega p(\nabla \cdot \mathbf{v})\, dxdy &= \int_\Omega \mathbf{f} \cdot \mathbf{v}\, dxdy, \forall \mathbf{v} \in H_0^1(\Omega) \times H_0^1(\Omega), \\ - \int_\Omega (\nabla \cdot \mathbf{u}) q\, dxdy &= 0, \forall q \in L^2(\Omega), \end{aligned}$$

where,

$$\begin{aligned} &\mathbb{D}(\mathbf{u}) : \mathbb{D}(\mathbf{v}) \\ =&\frac{\partial u_1}{\partial x}\frac{\partial v_1}{\partial x} + \frac{\partial u_2}{\partial y}\frac{\partial v_2}{\partial y} + \frac{1}{2}\frac{\partial u_1}{\partial y}\frac{\partial v_1}{\partial y} + \frac{1}{2}\frac{\partial u_1}{\partial y}\frac{\partial v_2}{\partial x} + \frac{1}{2}\frac{\partial u_2}{\partial x}\frac{\partial v_1}{\partial y} + \frac{1}{2}\frac{\partial u_2}{\partial x}\frac{\partial v_2}{\partial x}. \end{aligned}$$

Introducing bilinear form,

$$a(\mathbf{u}, \mathbf{v}) = \int_{\Omega} 2\nu\mathbb{D}(\mathbf{u}) : \mathbb{D}(\mathbf{v})\, dxdy,$$
$$b(\mathbf{u}, q) = -\int_{\Omega} (\nabla \cdot \mathbf{u}) q\, dxdy.$$

Then, the variational formulation of the mixed FEM of Eq (1.1) is to find $\mathbf{u} \in H_0^1(\Omega) \times H_0^1(\Omega)$ and $p \in L^2(\Omega)$, satisfying the following equation

$$\begin{cases} a(\mathbf{u}, \mathbf{v}) + b(\mathbf{v}, p) = (\mathbf{f}, \mathbf{v}), \\ b(\mathbf{u}, q) = 0, \end{cases} \tag{3.1}$$

for any $\mathbf{v} \in H_0^1(\Omega) \times H_0^1(\Omega)$ and $q \in L^2(\Omega)$, where $(\mathbf{f}, \mathbf{v}) = \int_{\Omega} \mathbf{f} \cdot \mathbf{v}\, dxdy$.

Then, we consider the discrete form of variational Eq (3.1).

3.2. Finite element discretization

Let Ω_h be a uniform rectangle partition of Ω, $\mathbf{h} = [h_1, h_2] = [\frac{1}{N_1}, \frac{1}{N_2}]$ is the mesh size, where N_1 and N_2 represent the number of subintervals on the x-axis and y-axis of quasi-uniform subdivision. For each $T \in \Omega_h$, the local finite element space $Q(T, m, n)$ is spanned by Bernstein polynomial basis defined on T, i.e.,

$$Q(T, m, n) = \left\{ v, v \in span\left\{ B_{i,j}^{m,n}(s, \tau) \right\} \right\}.$$

Consider a finite element space $U_h(m, n) \subset H^1(\Omega)$ for the velocity $\mathbf{u}$ and a finite element space $W_h(h, l) \subset L^2(\Omega)$ for the pressure p. Assume that the polynomial space in the construction of U_h contains $P_k, k \geq 1$ and that of W_h contains P_{k-1}, where,

$$U_h(m, n) = \{ r, r \in Q(T, m, n), \forall T \in \Omega_h \},$$
$$W_h(h, l) = \{ w, w \in Q(T, h, l), \forall T \in \Omega_h \}.$$

Define U_{h0} to be the space that consists of the functions of U_h with vanishing boundary values.

Subsequently, the discrete scheme of Eq (3.1) is to find $\mathbf{u}_h \in U_h \times U_h$ and $p_h \in W_h$, where $\mathbf{u}_h = (u_{1h}, u_{2h})$ such that

$$\begin{cases} a(\mathbf{u}_h, \mathbf{v}_h) + b(\mathbf{v}_h, p_h) = (\mathbf{f}, \mathbf{v}_h), \\ b(\mathbf{u}_h, q_h) = 0, \end{cases} \tag{3.2}$$

for any $\mathbf{v}_h \in U_{h0} \times U_{h0}$ and $q_h \in W_h$.

In order to verify if $\mathbf{v}_h$ and q_h satisfy the inf-sup condition, we now define an interpolation π_h so that it is a modification of B_h, that is, satisfying $\pi_h \mathbf{u} = B_h(\mathbf{u})$. From (2.4), we know π_h is bounded. Discrete compatibility is similar to that proved in [48], that is, $b(\mathbf{u} - \pi_h \mathbf{u}, q) = 0$. So, $\mathbf{v}_h$ and q_h satisfy the following inf-sup condition:

$$\inf_{0 \neq q_h \in W_h} \sup_{0 \neq \mathbf{v}_h \in U_{h0} \times U_{h0}} \frac{b(\mathbf{v}_h, q_h)}{\|\nabla \mathbf{v}_h\|_0 \, \|q_h\|_0} > \beta,$$

where $\beta > 0$ is a constant independent of mesh size h.

In the scalar format, Eq (3.2) is to find $u_{1h} \in U_h, u_{2h} \in U_h$, and $p_h \in W_h$ such that

$$\begin{aligned}
&\int_\Omega \nu\Big(2\frac{\partial u_{1h}}{\partial x}\frac{\partial v_{1h}}{\partial x} + 2\frac{\partial u_{2h}}{\partial y}\frac{\partial v_{2h}}{\partial y} + \frac{\partial u_{1h}}{\partial y}\frac{\partial v_{1h}}{\partial y} \\
&+\frac{\partial u_{1h}}{\partial y}\frac{\partial v_{2h}}{\partial x} + \frac{\partial u_{2h}}{\partial x}\frac{\partial v_{1h}}{\partial y} + \frac{\partial u_{2h}}{\partial x}\frac{\partial v_{2h}}{\partial x}\Big)dxdy \\
&- \int_\Omega \left(p_h\frac{\partial v_{1h}}{\partial x} + p_h\frac{\partial v_{2h}}{\partial y}\right)dxdy \\
&= \int_\Omega (f_1 v_{1h} + f_2 v_{2h})dxdy \\
&- \int_\Omega \left(\frac{\partial u_{1h}}{\partial x}q_h + \frac{\partial u_{2h}}{\partial y}q_h\right)dxdy = 0,
\end{aligned} \tag{3.3}$$

for any $v_{1h} \in U_h, v_{2h} \in U_h, q_h \in W_h$.

Since $u_{1h},\ u_{2h} \in U_h = span\{r_j\}_{j=1}^{N_b}$ and $p_h \in W_h = span\{w_j\}_{j=1}^{N_{bp}}$, then

$$u_{1h} = \sum_{j=1}^{N_b} u_{1j}r_j, \quad u_{2h} = \sum_{j=1}^{N_b} u_{2j}r_j, \quad p_h = \sum_{j=1}^{N_{bp}} p_j w_j,$$

for some coefficients $u_{1j},\ u_{2j}(j = 1, \cdots, N_b)$, and $p_j(j = 1, \cdots, N_{bp})$.

Now, we set up a linear algebraic system for $u_{1j}, u_{2j}(j = 1, \cdots, N_b)$ and $p_j(j = 1, \cdots, N_{bp})$. Then we can solve it to obtain the finite element solution $\mathbf{u}_h = (u_{1h}, u_{2h})^t$ and p_h.

For the first equation in the Eq (3.3), in the first set of test functions, we set $\mathbf{v}_h = (r_i, 0)^t$, namely, $v_{1h} = r_i(i = 1, \cdots, N_b)$ and $v_{2h} = 0$. Then

$$\begin{aligned}
&2\int_\Omega \nu\left(\sum_{j=1}^{N_b} u_{1j}\frac{\partial r_j}{\partial x}\right)\frac{\partial r_i}{\partial x}dxdy + \int_\Omega \nu\left(\sum_{j=1}^{N_b} u_{1j}\frac{\partial r_j}{\partial y}\right)\frac{\partial r_i}{\partial y}dxdy \\
&+ \int_\Omega \nu\left(\sum_{j=1}^{N_b} u_{2j}\frac{\partial r_j}{\partial x}\right)\frac{\partial r_i}{\partial y}dxdy - \int_\Omega \left(\sum_{j=1}^{N_{bp}} p_j w_j\right)\frac{\partial r_i}{\partial x}dxdy \\
&= \int_\Omega f_1 r_i dxdy.
\end{aligned}$$

After that, we let $\mathbf{v}_h = (0, r_i)^t$, i.e., $v_{1h} = 0$ and $v_{2h} = r_i(i = 1, \cdots, N_b)$,

$$\begin{aligned}
&2\int_\Omega \nu\left(\sum_{j=1}^{N_b} u_{2j}\frac{\partial r_j}{\partial y}\right)\frac{\partial r_i}{\partial y}dxdy + \int_\Omega \nu\left(\sum_{j=1}^{N_b} u_{1j}\frac{\partial r_j}{\partial y}\right)\frac{\partial r_i}{\partial x}dxdy \\
&+ \int_\Omega \nu\left(\sum_{j=1}^{N_b} u_{2j}\frac{\partial r_j}{\partial x}\right)\frac{\partial r_i}{\partial x}dxdy - \int_\Omega \left(\sum_{j=1}^{N_{bp}} p_j w_j\right)\frac{\partial r_i}{\partial y}dxdy \\
&= \int_\Omega f_2 r_i dxdy.
\end{aligned}$$

Lastly, set $q_h = w_i(i = 1, \cdots, N_{bp})$ in the second equation of the Eq (3.3), getting

$$-\int_\Omega \left(\sum_{j=1}^{N_b} u_{1j}\frac{\partial r_j}{\partial x}\right)w_i dxdy - \int_\Omega \left(\sum_{j=1}^{N_b} u_{2j}\frac{\partial r_j}{\partial y}\right)w_i dxdy = 0.$$

Simplify the above three sets of equations, obtaining

$$\sum_{j=1}^{N_b} u_{1j}\left(2\int_\Omega \nu\frac{\partial r_j}{\partial x}\frac{\partial r_i}{\partial x}dxdy+\int_\Omega \nu\frac{\partial r_j}{\partial y}\frac{\partial r_i}{\partial y}dxdy\right)$$
$$+\sum_{j=1}^{N_b} u_{2j}\left(\int_\Omega \nu\frac{\partial r_j}{\partial x}\frac{\partial r_i}{\partial y}dxdy\right)+\sum_{j=1}^{N_{bp}} p_j\left(-\int_\Omega w_j\frac{\partial r_i}{\partial x}dxdy\right)=\int_\Omega f_1 r_i dxdy,$$
$$\sum_{j=1}^{N_b} u_{1j}\left(\int_\Omega \nu\frac{\partial r_j}{\partial y}\frac{\partial r_i}{\partial x}dxdy\right)$$
$$+\sum_{j=1}^{N_b} u_{2j}\left(2\int_\Omega \nu\frac{\partial r_j}{\partial y}\frac{\partial r_i}{\partial y}dxdy+\int_\Omega \nu\frac{\partial r_j}{\partial x}\frac{\partial r_i}{\partial x}dxdy\right)$$
$$+\sum_{j=1}^{N_{bp}} p_j\left(-\int_\Omega w_j\frac{\partial r_i}{\partial y}dxdy\right)=\int_\Omega f_2 r_i dxdy,$$
$$\sum_{j=1}^{N_b} u_{1j}\left(-\int_\Omega \frac{\partial r_j}{\partial x}w_i dxdy\right)+\sum_{j=1}^{N_b} u_{2j}\left(-\int_\Omega \frac{\partial r_j}{\partial y}w_i dxdy\right)+\sum_{j=1}^{N_{bp}} p_j\cdot 0=0.$$

Define the stiffness matrix as

$$A=\begin{pmatrix} 2A_1+A_2 & A_3 & A_5 \\ A_4 & 2A_2+A_1 & A_6 \\ A_7 & A_8 & \mathbb{O} \end{pmatrix},$$

where $\mathbb{O}=[0]_{i=1,j=1}^{N_{bp},N_{bp}}$,

$$A_1=\left[\int_\Omega \nu\frac{\partial r_j}{\partial x}\frac{\partial r_i}{\partial x}dxdy\right]_{i,j=1}^{N_b},\quad A_2=\left[\int_\Omega \nu\frac{\partial r_j}{\partial y}\frac{\partial r_i}{\partial y}dxdy\right]_{i,j=1}^{N_b},$$
$$A_3=\left[\int_\Omega \nu\frac{\partial r_j}{\partial x}\frac{\partial r_i}{\partial y}dxdy\right]_{i,j=1}^{N_b},\quad A_4=\left[\int_\Omega \nu\frac{\partial r_j}{\partial y}\frac{\partial r_i}{\partial x}dxdy\right]_{i,j=1}^{N_b},$$
$$A_5=\left[\int_\Omega -w_j\frac{\partial r_i}{\partial x}dxdy\right]_{i=1,j=1}^{N_b,N_{bp}},\quad A_6=\left[\int_\Omega -w_j\frac{\partial r_i}{\partial y}dxdy\right]_{i=1,j=1}^{N_b,N_{bp}},$$
$$A_7=\left[\int_\Omega -\frac{\partial r_j}{\partial x}w_i dxdy\right]_{i=1,j=1}^{N_{bp},N_b},\quad A_8=\left[\int_\Omega -\frac{\partial r_j}{\partial y}w_i dxdy\right]_{i=1,j=1}^{N_{bp},N_b}.$$

Define the load vector

$$\vec{b}=\begin{pmatrix} \vec{b_1} \\ \vec{b_2} \\ \vec{0} \end{pmatrix},$$

where $\vec{0}=[0]_{i=1}^{N_{bp}}$,

$$\vec{b_1}=\left[\int_\Omega f_1 r_i dxdy\right]_{i=1}^{N_b},\ \vec{b_2}=\left[\int_\Omega f_2 r_i dxdy\right]_{i=1}^{N_b}.$$

Define the unknown vector

$$\vec{X} = \begin{pmatrix} \vec{X_1} \\ \vec{X_2} \\ \vec{X_3} \end{pmatrix},$$

where,

$$\vec{X_1} = [u_{1j}]_{j=1}^{N_b},\ \vec{X_2} = [u_{2j}]_{j=1}^{N_b},\ \vec{X_3} = [p_j]_{j=1}^{N_{bp}}.$$

Then, we get a linear system of ordinary differential equations for $u_{1j}, u_{2j}(j = 1, \cdots, N_b)$ and $p_j(j = 1, \cdots, N_{bp})$,

$$A\vec{X} = \vec{b}, \tag{3.4}$$

so we can solve system (3.4) and obtain the unknown vector group $\vec{X}$.

4. Numerical examples

In this section, we verify the feasibility and effectiveness of this method using several numerical examples. Tensor product Bernstein polynomial bases are used to construct the trial function space and test function space of the mixed FEM, the approximate solutions are solved by MATLAB2022b, and the error and convergence order of the exact solution and the finite element solution under L^∞, L^2, and H^1-semi norms are obtained. The numerical results obtained by solving Stokes equation with bilinear, biquadratic, and bicubic Lagrange basis functions are consistent with those obtained by using Bernstein polynomial basis with corresponding orders. Since using Lagrange basis functions of higher than bicubic order leads to the Runge phenomenon when solving the Stokes equations, we only present the error results of Bernstein polynomial basis.

Example 1. *Consider the following two-dimensional stokes equation with Dirichlet boundary in rectangular domain* $\Omega = [0, 1] \times [0, 1]$.

$$\begin{cases} -\nabla \cdot \mathbf{T}(\mathbf{u}(x, y), p(x, y)) = \mathbf{f}(x, y),\ (x, y) \in \Omega, \\ \nabla \cdot \mathbf{u}(x, y) = 0,\ (x, y) \in \Omega, \\ \mathbf{u}(x, y)|_{\partial\Omega} = 0, \end{cases} \tag{4.1}$$

where the exact solution $\mathbf{u} = (u_1, u_2)^t$ *is*

$$\begin{aligned} u_1(x, y) &= x^2(1 - x)^2(2y - 6y^2 + 4y^3), \\ u_2(x, y) &= -y^2(1 - y)^2(2x - 6x^2 + 4x^3), \end{aligned}$$

the exact solution $p(x, y)$ *is*

$$p(x, y) = x - x^2,$$

and the body force $\mathbf{f} = (f_1, f_2)^t$ *is*

$$\begin{aligned} f_1(x, y) =& \nu(2y(y - 1)^2(12x^2 - 12x + 2) - x^2(24y - 12)(x - 1)^2 \\ &+ y^2(2y - 2)(12x^2 - 12x + 2)) - 2x - 2\nu(2(x - 1)^2(4y^3 - 6y^2 + 2y) \\ &+ 2x^2(4y^3 - 6y^2 + 2y) + 4x(2x - 2)(4y^3 - 6y^2 + 2y)) + 1, \\ f_2(x, y) =& 2\nu(2(y - 1)^2(4x^3 - 6x^2 + 2x) + 2y^2(4x^3 - 6x^2 + 2x) \\ &+ 4y(2y - 2)(4x^3 - 6x^2 + 2x)) - \nu(2x(x - 1)^2(12y^2 - 12y + 2) \\ &- y^2(24x - 12)(y - 1)^2 + x^2(2x - 2)(12y^2 - 12y + 2)), \end{aligned}$$

where we set $\nu = 1$.

The domain Ω *is partitioned into uniform rectangles. Here, we use biquadratic, bicubic, and biquartic Bernstein polynomial basis to solve the Stokes Eq (4.1), and calculate the* L^∞, L^2, *and* H^1*-semi norms between the approximate solution and the exact solution. Tables 1 and 2 show the numerical errors for these kinds of basis functions in* L^∞, L^2, *and* H^1*-semi norms; the corresponding convergence orders are shown in Tables 3 and 4. The comparison of errors are shown in Figures* 1 *and* 2.

Table 1. The comparison of numerical errors of $\mathbf{u}$ in L^∞, L^2, and H^1-semi norms.

basis	h_1	h_2	$\|\|u-u_h\|\|_{L^\infty}$	$\|\|u-u_h\|\|_{L^2}$	$\|u-u_h\|_{H^1}$
biquadratic Bernstein	$\frac{1}{4}$	$\frac{1}{4}$	$2.5683e-04$	$2.2975e-04$	$1.3000e-03$
	$\frac{1}{8}$	$\frac{1}{8}$	$3.3051e-05$	$2.9674e-05$	$1.7101e-04$
	$\frac{1}{16}$	$\frac{1}{16}$	$4.4028e-06$	$3.7355e-06$	$2.1478e-05$
	$\frac{1}{32}$	$\frac{1}{32}$	$5.5386e-07$	$4.6772e-07$	$2.6875e-06$
bicubic Bernstein	$\frac{1}{4}$	$\frac{1}{4}$	$7.3008e-06$	$4.9632e-06$	$2.3383e-04$
	$\frac{1}{8}$	$\frac{1}{8}$	$4.4274e-07$	$3.0623e-07$	$2.8934e-05$
	$\frac{1}{16}$	$\frac{1}{16}$	$2.6941e-08$	$1.9059e-08$	$3.6060e-06$
	$\frac{1}{32}$	$\frac{1}{32}$	$1.6506e-09$	$1.1897e-09$	$4.5039e-07$
biquartic Bernstein	$\frac{1}{4}$	$\frac{1}{4}$	$2.1182e-12$	$6.8916e-13$	$2.2454e-11$
	$\frac{1}{8}$	$\frac{1}{8}$	$7.6057e-13$	$3.5117e-13$	$2.3499e-11$
	$\frac{1}{16}$	$\frac{1}{16}$	$3.5179e-13$	$1.7482e-13$	$2.3665e-11$
	$\frac{1}{32}$	$\frac{1}{32}$	$1.6601e-13$	$8.7608e-14$	$2.3789e-11$

Table 2. The comparison of numerical errors of p in L^∞, L^2, and H^1-semi norms.

basis	h_1	h_2	$\|p-p_h\|_{L^\infty}$	$\|p-p_h\|_{L^2}$	$\|p-p_h\|_{H^1}$
bilinear Bernstein	$\frac{1}{4}$	$\frac{1}{4}$	$1.0700e-02$	$1.0400e-02$	$1.4430e-01$
	$\frac{1}{8}$	$\frac{1}{8}$	$2.6000e-03$	$2.6000e-03$	$7.2200e-02$
	$\frac{1}{16}$	$\frac{1}{16}$	$6.5301e-04$	$6.5104e-04$	$3.6100e-02$
	$\frac{1}{32}$	$\frac{1}{32}$	$1.6289e-04$	$1.6276e-04$	$1.8000e-02$
biquadratic Bernstein	$\frac{1}{4}$	$\frac{1}{4}$	$2.3900e-05$	$7.1260e-06$	$1.5554e-04$
	$\frac{1}{8}$	$\frac{1}{8}$	$1.2875e-06$	$1.8008e-07$	$8.0360e-06$
	$\frac{1}{16}$	$\frac{1}{16}$	$6.6020e-08$	$4.9431e-09$	$4.8683e-07$
	$\frac{1}{32}$	$\frac{1}{32}$	$3.5086e-09$	$1.8548e-10$	$4.8902e-08$
bicubic Bernstein	$\frac{1}{4}$	$\frac{1}{4}$	$2.8915e-10$	$1.2332e-10$	$4.8600e-09$
	$\frac{1}{8}$	$\frac{1}{8}$	$2.6243e-10$	$1.1638e-10$	$9.6834e-09$
	$\frac{1}{16}$	$\frac{1}{16}$	$2.4346e-10$	$1.1637e-10$	$1.9344e-08$
	$\frac{1}{32}$	$\frac{1}{32}$	$1.5440e-09$	$1.2847e-09$	$3.8696e-08$

Table 3. Convergence order under three norms of $\mathbf{u}$.

basis	$h/(\frac{1}{2}h)$	$L^\infty - order$	$L^2 - order$	$H^1 - order$
biquadratic Bernstein	$\frac{1}{4}/\frac{1}{8}$	2.9580	2.9528	2.9264
	$\frac{1}{8}/\frac{1}{16}$	2.9082	2.9898	2.9931
	$\frac{1}{16}/\frac{1}{32}$	2.9908	2.9976	2.9985
bicubic Bernstein	$\frac{1}{4}/\frac{1}{8}$	4.0435	3.6940	3.0146
	$\frac{1}{8}/\frac{1}{16}$	4.0386	4.0061	3.0043
	$\frac{1}{16}/\frac{1}{32}$	4.0287	4.0018	3.0012

Table 4. Convergence order under three norms of p.

basis	$h/(\frac{1}{2}h)$	$L^\infty - order$	$L^2 - order$	$H^1 - order$
bilinear Bernstein	$\frac{1}{4}/\frac{1}{8}$	2.0410	2.0000	0.9990
	$\frac{1}{8}/\frac{1}{16}$	1.9933	1.9977	1.0000
	$\frac{1}{16}/\frac{1}{32}$	2.0032	2.0000	1.0040
biquadratic Bernstein	$\frac{1}{4}/\frac{1}{8}$	4.2144	5.3064	4.2747
	$\frac{1}{8}/\frac{1}{16}$	4.2855	5.1871	4.0450
	$\frac{1}{16}/\frac{1}{32}$	4.2339	4.7361	3.3154

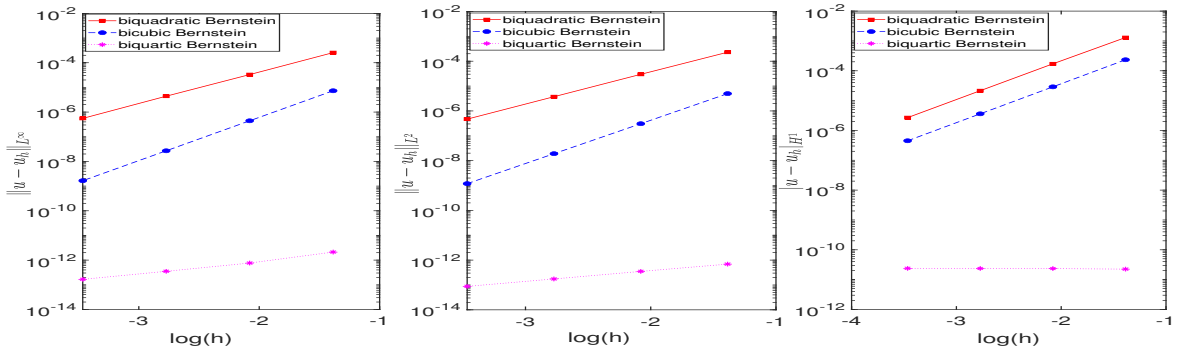

Figure 1. Error comparison of $u - u_h$ under L^∞, L^2, and H^1 norm.

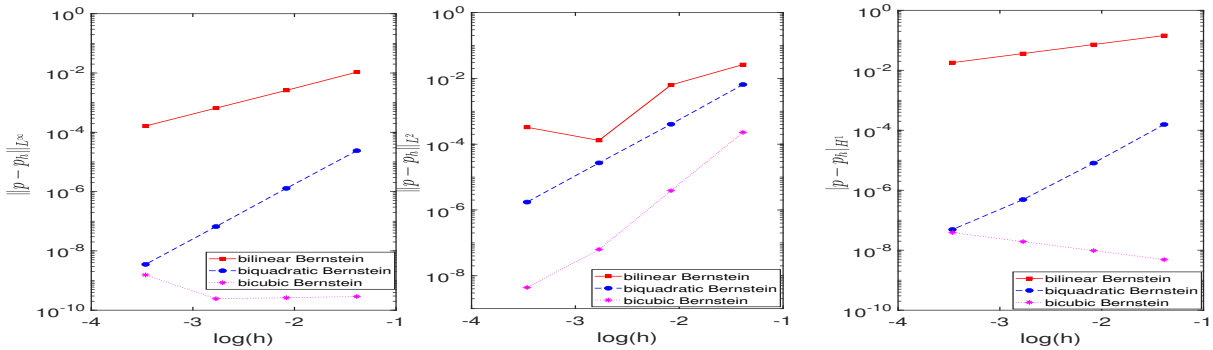

Figure 2. Error comparison of $p - p_h$ under L^∞, L^2, and H^1 norm.

When solving 2D Stokes equations, with equal mesh sizes, for velocity **u**, *the numerical accuracy of the bicubic Bernstein polynomial basis is* 1 *and* 2 *orders of magnitude higher than that of the biquadratic Bernstein polynomial basis, while the biquartic Bernstein polynomial basis is* 4–7 *orders of magnitude higher than the bicubic. For pressure p, the numerical accuracy of the biquadratic Bernstein polynomial basis is* 3–5 *orders of magnitude higher than that of the bilinear Bernstein polynomial basis, and the bicubic Bernstein polynomial basis is* 1–5 *orders of magnitude higher than*

the biquadratic.

When solving Eq (4.1) using biquartic Bernstein polynomial basis for velocity $\mathbf{u}$ *and bicubic Bernstein polynomial basis for pressure* p*, we attempted many methods, including adjusting the accuracy setting of MATLAB*2022*b to improve the accuracy and convergence order of the mixed FEM, but the effect was not obvious due to the limitation of computer hardware, so the convergence order could not be computed. In the future, we will continue to explore ways to improve performance.*

Example 2. *Consider the following Stokes equation*

$$\begin{cases} -\nabla \cdot \mathbf{T}(\mathbf{u}(x,y), p(x,y)) = \mathbf{f}(x,y), \ (x,y) \in \Omega, \\ \nabla \cdot \mathbf{u}(x,y) = 0, \ (x,y) \in \Omega, \\ \mathbf{u}(x,y)|_{\partial\Omega} = 0, \end{cases} \tag{4.2}$$

where $\Omega = [0,1] \times [0,1]$*, the exact solution* $\mathbf{u} = (u_1, u_2)^t$ *is*

$$\begin{aligned} u_1(x,y) &= -cos2\pi x sin2\pi y + sin2\pi y, \\ u_2(x,y) &= sin2\pi x cos2\pi y - sin2\pi x, \end{aligned}$$

the exact solution $p(x,y)$ *is*

$$p(x,y) = x^2 + y^2,$$

and the body force $\mathbf{f} = (f_1, f_2)^t$ *is*

$$\begin{aligned} f_1(x,y) =& 2x + 4\nu\pi^2 sin(2\pi y) - 8\nu\pi^2 cos(2\pi x) sin(2\pi y), \\ f_2(x,y) =& 2y - 4\nu\pi^2 sin(2\pi x) + 8\nu\pi^2 cos(2\pi y) sin(2\pi x), \end{aligned}$$

where we set $\nu = 1$.

Analogous to Example 1*, mixed FEM with bivariate Bernstein polynomial basis are used to solve the above problems. The numerical errors in* L^∞*,* L^2*, and* H^1*-semi norms are listed in Tables 5 and 6. The corresponding convergence orders are shown in Tables 7 and 8. Figures* 3 *and* 4 *display the error image.*

Table 5. The comparison of numerical errors of **u** in L^∞, L^2, and H^1-semi norms.

basis	h_1	h_2	$\|u-u_h\|_{L^\infty}$	$\|u-u_h\|_{L^2}$	$\|u-u_h\|_{H^1}$
biquadratic Bernstein	$\frac{1}{2}$	$\frac{1}{2}$	$1.6174e-01$	$1.5937e-01$	$2.3473e-00$
	$\frac{1}{4}$	$\frac{1}{4}$	$5.0100e-02$	$3.8000e-02$	$3.2450e-01$
	$\frac{1}{8}$	$\frac{1}{8}$	$7.6000e-03$	$5.3000e-03$	$4.2000e-02$
	$\frac{1}{16}$	$\frac{1}{16}$	$9.7064e-04$	$6.8074e-04$	$5.3000e-03$
bicubic Bernstein	$\frac{1}{2}$	$\frac{1}{2}$	$6.4761e-02$	$3.8419e-02$	$9.7374e-01$
	$\frac{1}{4}$	$\frac{1}{4}$	$4.6000e-03$	$2.2000e-03$	$1.0640e-01$
	$\frac{1}{8}$	$\frac{1}{8}$	$3.8009e-04$	$1.4194e-04$	$1.3500e-02$
	$\frac{1}{16}$	$\frac{1}{16}$	$2.5417e-05$	$8.9279e-06$	$1.7000e-03$
biquartic Bernstein	$\frac{1}{2}$	$\frac{1}{2}$	$5.8918e-03$	$3.8720e-03$	$1.1391e-01$
	$\frac{1}{4}$	$\frac{1}{4}$	$4.4542e-04$	$2.9417e-04$	$2.3000e-03$
	$\frac{1}{8}$	$\frac{1}{8}$	$1.4655e-05$	$9.4296e-06$	$7.2741e-05$
	$\frac{1}{16}$	$\frac{1}{16}$	$4.5821e-07$	$2.9652e-07$	$2.2833e-06$
biquintic Bernstein	$\frac{1}{2}$	$\frac{1}{2}$	$1.1305e-03$	$7.5132e-04$	$3.0851e-02$
	$\frac{1}{4}$	$\frac{1}{4}$	$2.7425e-05$	$1.9000e-05$	$1.4613e-04$
	$\frac{1}{8}$	$\frac{1}{8}$	$6.3294e-07$	$3.0283e-07$	$2.3289e-06$
	$\frac{1}{16}$	$\frac{1}{16}$	$1.0992e-08$	$4.7554e-09$	$3.7396e-08$

Table 6. The comparison of numerical errors of p in L^∞, L^2, and H^1-semi norms.

basis	h_1	h_2	$\|p - p_h\|_{L^\infty}$	$\|p - p_h\|_{L^2}$	$\|p - p_h\|_{H^1}$
bilinear Bernstein	$\frac{1}{2}$	$\frac{1}{2}$	$1.1055e-01$	$8.7401e-02$	$4.0825e-01$
	$\frac{1}{4}$	$\frac{1}{4}$	$5.2700e-02$	$2.6300e-02$	$2.7690e-01$
	$\frac{1}{8}$	$\frac{1}{8}$	$1.3800e-02$	$6.3000e-03$	$1.0890e-01$
	$\frac{1}{16}$	$\frac{1}{16}$	$2.0000e-03$	$1.3000e-03$	$5.1100e-02$
biquadratic Bernstein	$\frac{1}{2}$	$\frac{1}{2}$	$3.0446e-01$	$1.5070e-01$	$1.7746e-00$
	$\frac{1}{4}$	$\frac{1}{4}$	$1.6700e-02$	$6.5000e-03$	$1.7270e-01$
	$\frac{1}{8}$	$\frac{1}{8}$	$9.8603e-04$	$4.0417e-04$	$2.3900e-02$
	$\frac{1}{16}$	$\frac{1}{16}$	$7.6837e-05$	$2.6949e-05$	$3.3000e-03$
bicubic Bernstein	$\frac{1}{2}$	$\frac{1}{2}$	$2.0060e-02$	$7.7363e-03$	$1.4123e-01$
	$\frac{1}{4}$	$\frac{1}{4}$	$5.0825e-04$	$2.2814e-04$	$7.5000e-03$
	$\frac{1}{8}$	$\frac{1}{8}$	$1.0791e-05$	$3.8490e-06$	$2.4536e-04$
	$\frac{1}{16}$	$\frac{1}{16}$	$1.8552e-07$	$6.3212e-08$	$7.9160e-06$
biquartic Bernstein	$\frac{1}{2}$	$\frac{1}{2}$	$3.9974e-03$	$2.3690e-03$	$7.2008e-02$
	$\frac{1}{4}$	$\frac{1}{4}$	$2.9541e-05$	$1.1172e-05$	$6.0166e-04$
	$\frac{1}{8}$	$\frac{1}{8}$	$2.1714e-07$	$7.5228e-08$	$8.0550e-06$
	$\frac{1}{16}$	$\frac{1}{16}$	$1.2925e-08$	$3.3008e-09$	$8.7917e-07$

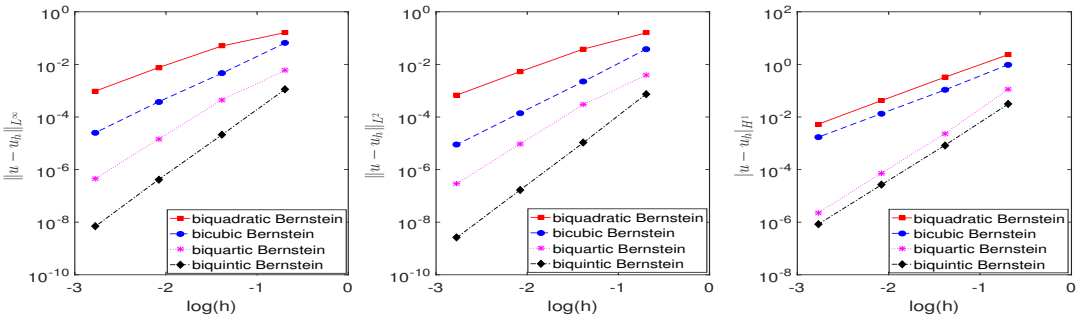

Figure 3. Error comparison of $u - u_h$ under L^∞, L^2, and H^1 norm.

Table 7. Convergence order under three norms of **u**.

basis	$h/(\frac{1}{2}h)$	$L^\infty - order$	$L^2 - order$	$H^1 - order$
biquadratic Bernstein	$\frac{1}{2}/\frac{1}{4}$	1.6908	2.0683	2.8547
	$\frac{1}{4}/\frac{1}{8}$	2.7207	2.8419	2.9498
	$\frac{1}{8}/\frac{1}{16}$	2.9690	2.9608	2.7866
bicubic Bernstein	$\frac{1}{2}/\frac{1}{4}$	3.8154	4.1262	3.1940
	$\frac{1}{4}/\frac{1}{8}$	3.5972	3.9542	2.9785
	$\frac{1}{8}/\frac{1}{16}$	3.9025	3.9908	2.9894
biquartic Bernstein	$\frac{1}{2}/\frac{1}{4}$	3.7255	3.7184	5.6301
	$\frac{1}{4}/\frac{1}{8}$	4.9257	4.9633	4.9827
	$\frac{1}{8}/\frac{1}{16}$	4.9992	4.9910	4.9936
biquintic Bernstein	$\frac{1}{2}/\frac{1}{4}$	5.7603	6.1691	5.2112
	$\frac{1}{4}/\frac{1}{8}$	5.6375	5.9800	4.9813
	$\frac{1}{8}/\frac{1}{16}$	5.9043	5.9930	4.9953

Table 8. Convergence order under three norms of p.

basis	$h/(\frac{1}{2}h)$	$L^\infty - order$	$L^2 - order$	$H^1 - order$
bilinear Bernstein	$\frac{1}{2}/\frac{1}{4}$	1.0688	1.7326	0.5601
	$\frac{1}{4}/\frac{1}{8}$	1.9331	2.0616	1.3464
	$\frac{1}{8}/\frac{1}{16}$	2.7866	2.2768	1.0916
biquadratic Bernstein	$\frac{1}{2}/\frac{1}{4}$	4.1883	4.5351	3.3612
	$\frac{1}{4}/\frac{1}{8}$	4.0821	4.0074	2.8532
	$\frac{1}{8}/\frac{1}{16}$	3.6818	3.9067	2.8565
bicubic Bernstein	$\frac{1}{2}/\frac{1}{4}$	5.3026	5.0837	4.2350
	$\frac{1}{4}/\frac{1}{8}$	5.5576	5.8893	4.9339
	$\frac{1}{8}/\frac{1}{16}$	5.8621	5.9281	4.9540
biquartic Bernstein	$\frac{1}{2}/\frac{1}{4}$	5.5209	6.2951	5.0997
	$\frac{1}{4}/\frac{1}{8}$	5.8011	5.9533	4.8669
	$\frac{1}{8}/\frac{1}{16}$	5.1332	5.3535	4.4198

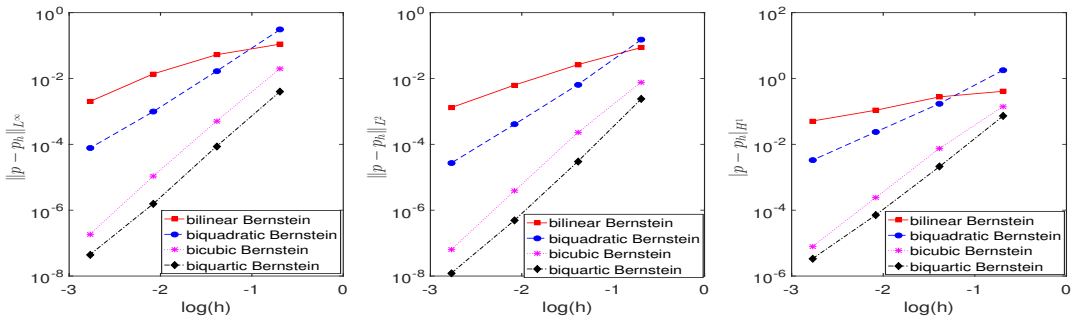

Figure 4. Error comparison of $p - p_h$ under L^∞, L^2, and H^1 norm.

It can be observed from the error line in Figures 3 *and* 4*, and the error convergence order in Tables* 7 *and* 8 *that when the mesh size is equal, the higher the degree of Bernstein polynomial basis, not only the higher the numerical accuracy of the error norm, but also the higher the error convergence order.*

Example 3. *Consider the following non-homogenous* 2*D Stokes equation*

$$\begin{cases} -\nabla \cdot \mathbf{T}(\mathbf{u}(x,y), p(x,y)) = \mathbf{f}(x,y), \ (x,y) \in \Omega, \\ \nabla \cdot \mathbf{u}(x,y) = 0, \ (x,y) \in \Omega, \\ \mathbf{u}(x,y)|_{\partial\Omega} = g, \end{cases} \tag{4.3}$$

where $\Omega = [0,1] \times [0,1]$*, the exact solution* $\mathbf{u} = (u_1, u_2)^t$ *is*

$$u_1(x,y) = \pi sin\pi x cos\pi y,$$
$$u_2(x,y) = -\pi cos\pi x sin\pi y,$$

the exact solution $p(x,y)$ *is*

$$p(x,y) = sin\pi x sin\pi y,$$

and the body force $\mathbf{f} = (f_1, f_2)^t$ *is*

$$f_1(x,y) = 2\nu\pi^3 cos(\pi y)sin(\pi x) + \pi cos\pi x sin\pi y,$$
$$f_2(x,y) = -2\nu\pi^3 cos(\pi x)sin(\pi y) + \pi cos\pi y sin\pi x,$$

where we set $\nu = 1$.

We continue to use the above method to solve Stokes Eq (4.3). The numerical errors are shown in Tables 9 *and* 10.

Table 9. The comparison of numerical errors of $\mathbf{u}$ in L^∞, L^2, and H^1-semi norms.

Bernstein basis	h_1	h_2	$\|u - u_h\|_{L^\infty}$	$\|\mathbf{u} - \mathbf{u}_h\|_{L^2}$	$\|\mathbf{u} - \mathbf{u}_h\|_{H^1}$
biquadratic for $\mathbf{u}$	$\frac{1}{4}$	$\frac{1}{4}$	$7.1700e-02$	$4.5300e-02$	$3.0170e-01$
	$\frac{1}{8}$	$\frac{1}{8}$	$1.8600e-02$	$1.0600e-02$	$7.6200e-02$
bilinear for p	$\frac{1}{16}$	$\frac{1}{16}$	$4.8000e-03$	$2.6000e-03$	$1.9100e-02$
	$\frac{1}{32}$	$\frac{1}{32}$	$1.2000e-03$	$6.4904e-04$	$4.8000e-03$
bicubic for $\mathbf{u}$	$\frac{1}{4}$	$\frac{1}{4}$	$5.8200e-02$	$2.7800e-02$	$2.4340e-01$
	$\frac{1}{8}$	$\frac{1}{8}$	$1.5600e-02$	$6.9000e-03$	$7.9500e-02$
bilinear for p	$\frac{1}{16}$	$\frac{1}{16}$	$4.0000e-03$	$1.7000e-03$	$2.6800e-02$
	$\frac{1}{32}$	$\frac{1}{32}$	$1.0000e-03$	$4.3277e-04$	$9.2000e-03$

As can be seen from Tables 9 *and* 10*, the Bernstein basis function shows good convergence under the three norms as the grid size decreases, which further verifies its advantages in numerical stability. In particular, the cubic or higher-degree Lagrange interpolation shows unstable oscillations, while the Bernstein basis function can provide a stable and consistent solution, while maintaining good geometric properties and flexible boundary condition processing capabilities. The numerical stability and global approximation characteristics of Bernstein polynomial make the results more reliable than Lagrange interpolation.*

The Stokes equations are primarily used to describe fluid flow phenomena at low Re, where the inertial forces are significantly smaller compared to the viscous forces and can thus be neglected. This results in a flow that is smooth and orderly. Through the three numerical experiments presented above, we observe that as the mesh size decreases, the errors also gradually diminish. This indicates that our numerical solutions are progressively approaching the true laminar flow state. This trend demonstrates the effectiveness and accuracy of our numerical method in handling low Re fluid dynamics problems.

Table 10. The comparison of numerical errors of p in L^∞, L^2, and H^1-semi norms.

Bernstein basis	h_1	h_2	$\|p - p_h\|_{L^\infty}$	$\|p - p_h\|_{L^2}$	$\|p - p_h\|_{H^1}$
biquadratic for **u**	$\frac{1}{4}$	$\frac{1}{4}$	$9.5200e-02$	$4.5800e-02$	$5.7360e-01$
	$\frac{1}{8}$	$\frac{1}{8}$	$2.7400e-02$	$1.0700e-02$	$1.6570e-01$
bilinear for p	$\frac{1}{16}$	$\frac{1}{16}$	$7.5000e-03$	$2.6000e-03$	$6.0500e-02$
	$\frac{1}{32}$	$\frac{1}{32}$	$2.0000e-03$	$6.6176e-04$	$2.6800e-02$
bicubic for **u**	$\frac{1}{4}$	$\frac{1}{4}$	$8.7900e-02$	$3.0400e-02$	$4.0270e-01$
	$\frac{1}{8}$	$\frac{1}{8}$	$2.1600e-02$	$7.3000e-03$	$1.3450e-01$
bilinear for p	$\frac{1}{16}$	$\frac{1}{16}$	$5.5000e-03$	$1.8000e-03$	$5.5500e-02$
	$\frac{1}{32}$	$\frac{1}{32}$	$1.4000e-03$	$4.5304e-04$	$2.6100e-02$

In this study, we use tensor product Bernstein polynomial basis function and Lagrange basis function to solve Stokes equation and verify the basis functions of different orders in detail. The results show that the solutions obtained by using bicubic or low-order Lagrange basis functions are basically the same as those obtained by using Bernstein polynomial basis functions in numerical accuracy and convergence order, with slight differences only after the decimal point of some p values, but the performance of Bernstein basis functions is slightly better overall. This shows that the performance of the two basis functions is equivalent in the case of lower order, but Bernstein basis function shows better stability in detail processing.

However, when the biquartic Lagrange basis function is used to solve the problem, the situation has changes significantly. In Example 1, the error result of biquartic Lagrange basis function is not as good as that of biquartic Lagrange basis function. In Examples 2 and 3, the solution of biquartic Lagrange basis function appears an obvious oscillation phenomenon, which leads to unreliable numerical results. This phenomenon shows that with the increase of the order of the basis function, and with Lagrange basis function being prone to numerical instability when dealing with complex problems, especially in the case of high order, this instability will be aggravated. In contrast, Bernstein basis functions show excellent numerical stability and higher accuracy in high-order cases. By using high-order Bernstein polynomial basis, we not only effectively alleviate the oscillation problem caused by high-order Lagrange basis function, but also generate more stable and accurate numerical solutions. Therefore, in order to ensure the reliability and stability of numerical results, we only show the solution results using Bernstein polynomial basis functions.

5. Conclusions

We review the Bernstein polynomial basis and use it to construct the mixed finite element function space. Then, the Galerkin mixed FEM based on the bivariate Bernstein polynomial basis is used to solve the 2D Stokes equation, and the L^∞, L^2, and H^1-semi norms of the error and convergence order between the exact solution and the finite element solution are calculated. At the same time,

compared with the Lagrange basis function, the numerical accuracy and convergence order of solving Stokes equation with bicubic and below Lagrange interpolation polynomial basis and Bernstein polynomial basis are the same. High-order Lagrange interpolation function is often limited by Runge's phenomenon, so we use high-order Bernstein polynomial basis to effectively overcome this problem and obtain significantly better numerical results.

Author contributions

Lanyin Sun: Writing-review & editing, methodology, funding acquisition, conceptualization, visualization, data curation; Siya Wen: Writing-review & editing, writing-original draft, software. All authors have read and approved the final version of the manuscript for publication.

Use of Generative-AI tools declaration

The authors declare they have not used Artificial Intelligence (AI) tools in the creation of this article.

Acknowledgments

The authors are very grateful to the editor and anonymous referees for their valuable comments and constructive suggestions, which helped to improve the paper significantly. This work is partly supported by Program for Science Technology Innovation Talents in Universities of Henan Province (No. 22HASTIT021), the Science and Technology Project of Henan Province (No. 212102210394).

Conflict of interest

The authors declare that there is no conflict of interest.

References

1. B. J. Gireesha, K. J. Gowtham, Efficient hypergeometric wavelet approach for solving lane-emden equations, *J. Comput. Sci.*, **82** (2024), 1–11. http://dx.doi.org/10.1016/j.jocs.2024.102392
2. G. K. Ramesh, B. J. Gireesha, Non-linear radiative flow of nanofluid past a moving/stationary Riga plate, *Front. Heat Mass Tran.*, **9** (2017), 1–7. http://dx.doi.org/10.5098/hmt.9.3
3. W. Layton, *Introduction to the numerical analysis of incompressible viscous flows*, SIAM, 2008.
4. Q. Du, X. Tian, Mathematics of smoothed particle hydrodynamics: A study via nonlocal Stokes equations, *Found. Comput. Math.*, **20** (2020), 801–826. http://dx.doi.org/10.1007/s10208-019-09432-0
5. T. Borrvall, J. Petersson, Topology optimization of fluids in Stokes flow, *Int. J. Numer. Meth. Fl.*, **41** (2003), 77–107. http://dx.doi.org/10.1002/fld.426
6. L. E. Payne, W. H. Pell, The Stokes flow problem for a class of axially symmetric bodies, *J. Fluid Mech.*, **7** (1960), 529–549. http://dx.doi.org/10.1017/s002211206000027x

7. B. Andrea, D. Alan, L. Martin, A divergence-conforming finite element method for the surface Stokes equation, *SIAM J. Numer. Anal.*, **58** (2020), 2764–2798. http://dx.doi.org/10.1137/19M1284592
8. P. B. Bochev, M. D. Gunzburger, Analysis of least squares finite element methods for the Stokes equations, *Math. Comput.*, **63** (1994), 479–506. http://dx.doi.org/10.1090/s0025-5718-1994-1257573-4
9. J. Wang, X. Ye, A weak Galerkin finite element method for the Stokes equations, *Adv. Comput. Math.*, **42** (2016), 155–174. http://dx.doi.org/10.1007/s10444-015-9415-2
10. M. Shao, L. Song, P. Li, A generalized finite difference method for solving Stokes interface problems, *Eng. Anal. Bound. Elem.*, **132** (2021), 50–64. http://dx.doi.org/10.1016/j.enganabound.2021.07.002
11. R. Stenberg, M. Suri, Mixed finite element methods for problems in elasticity and Stokes flow, *Numer. Math.*, **72** (1996), 367–389. http://dx.doi.org/10.1007/s002110050174
12. A. Zeb, L. Elliott, D. B. Ingham, D. Lesnic, The boundary element method for the solution of Stokes equations in two-dimensional domains, *Eng. Anal. Bound. Elem.*, **22** (1998), 317–326. http://dx.doi.org/10.1016/s0955-7997(98)00072-1
13. B. Reidinger, O. Steinbach, A symmetric boundary element method for the Stokes problem in multiple connected domains, *Math. Method. Appl. Sci.*, **26** (2003), 77–93. http://dx.doi.org/10.1002/mma.347
14. J. Walter, A. V. Salsac, D. B. Biesel, P. L. Tallec, Coupling of finite element and boundary integral methods for a capsule in a Stokes flow, *Int. J. Numer. Meth. Eng.*, **83** (2010), 829–850. http://dx.doi.org/10.1002/nme.2859
15. P. Su, J. Chen, R. Yang, J. Xiang, A new isogeometric finite element method for analyzing structures, *CMES-Comp. Model. Eng.*, **141** (2024), 1883–1905. http://dx.doi.org/10.32604/CMES.2024.055942
16. A. Radu, C. Stan, D. Bejan, Finite element 3D model of a double quantum ring: Effects of electric and laser fields on the interband transition, *New J. Phys.*, **25** (2023), 1–20. http://dx.doi.org/10.1088/1367-2630/AD0B5F
17. G. Wei, P. Lardeur, F. Druesne, Free vibration analysis of thin to thick straight or curved beams by a solid-3D beam finite element method, *Thin Wall. Struct.*, **191** (2023), 1–16. http://dx.doi.org/10.1016/J.TWS.2023.111028
18. R. Courant, Variational methods for the solution of problems of equilibrium and vibrations, *B. Am. Math. Soc.*, **49** (1943), 1–23. https://doi.org/10.1090/S0002-9904-1943-07818-4
19. K. Feng, Difference schemes based on variational principle, *J. Appl. Comput. Math.*, **2** (1965), 238–262.
20. H. Huang, J. Wang, J. Cui, Difference scheme based on displacement solution on the plane elasticity, *J. Appl. Comput. Math.*, **3** (1966), 54–60.
21. C. Guichard, E. H. Quenjel, Weighted positive nonlinear finite volume method for dominated anisotropic diffusive equations, *Adv. Comput. Math.*, **48** (2022), 1–27. http://dx.doi.org/10.1007/s10444-022-09995-7

22. L. Zhang, S. Wang, G. Niu, Upwind finite element method for solving radiative heat transfer in graded index media, *Adv. Mater. Res.*, **1601** (2012), 1655–1658. http://dx.doi.org/10.4028/www.scientific.net/amr.430-432.1655

23. M. Puthukkudi, C. G. Raja, Mollification of fourier spectral methods with polynomial kernels, *Math. Method. Appl. Sci.*, **47** (2024), 4911–4931. http://dx.doi.org/10.1002/MMA.9845

24. Z. Csati, N. Moës, T. J. Massart, A stable extended/generalized finite element method with Lagrange multipliers and explicit damage update for distributed cracking in cohesive materials, *Comput. Methods Appl. M.*, **369** (2020), 1–50. http://dx.doi.org/10.1016/j.cma.2020.113173

25. Y. Tang, Z. Yin, Hermite finite element method for a class of viscoelastic beam vibration problem, *Engineering*, **13** (2021), 463–471. https://doi.org/10.4236/eng.2021.138033

26. C. Carstensen, J. Hu, Hierarchical Argyris finite element method for adaptive and multigrid algorithms, *Comput. Method. Appl. Math.*, **21** (2021), 529–556. http://dx.doi.org/10.1515/CMAM-2021-0083

27. M. I. Bhatti, P. Bracken, Solutions of differential equations in a Bernstein polynomial basis, *J. Comput. Appl. Math.*, **205** (2007), 272–280. http://dx.doi.org/10.1016/j.cam.2006.05.002

28. Z. Shi, On spline finite element method, *Math. Numer. Sinica*, **1** (1979), 50–72.

29. R. Qin, Simple formula for calculating stress intensity factor of fracture toughness samples, *Mech. Eng.*, **1** (1979), 52–53.

30. T. J. R. Hughes, J. A. Cottrell, Y. Bazilevs, Isogeometric analysis: CAD, finite elements, NURBS, exact geometry and mesh refinement, *Comput. Method. Appl. M.*, **194** (2005), 4135–4195. http://dx.doi.org/10.1016/j.cma.2004.10.008

31. C. Zhu, W. Kang, Numerical solution of Burgers-Fisher equation by cubic B-spline quasi-interpolation, *Appl. Math. Comput.*, **216** (2010), 2679–2686. http://dx.doi.org/10.1016/j.amc.2010.03.113

32. D. Dutykh, E. Pelinovsky, Numerical simulation of a solitonic gas in KdV and KdV-BBM equations, *Phys. Lett. A*, **378** (2014), 3102–3110. http://dx.doi.org/10.1016/j.physleta.2014.09.008

33. S. S. D. Pranta, H. Ali, M. S. Islam, On the numerical treatment of 2D nonlinear parabolic PDEs by the Galerkin method with bivariate Bernstein polynomial bases, *J. Appl. Math. Comput.*, **6** (2022), 410–422. http://dx.doi.org/10.26855/JAMC.2022.12.003

34. A. A. Rodríguez, L. B. Bruno, F. Rapetti, Whitney edge elements and the Runge phenomenon, *J. Comput. Appl. Math.*, **427** (2023), 1–9. http://dx.doi.org/10.1016/j.cam.2023.115117

35. S. Sindhu, B. J. Gireesha, Entropy generation analysis of hybrid nanofluid in a microchannel with slip flow, convective boundary and nonlinear heat flux, *Int. J. Numer. Meth. Fl.*, **31** (2021), 53–74. http://dx.doi.org/10.1108/hff-02-2020-0096

36. A. Felicita, B. J. Gireesha, B. Nagaraja, P. Venkatesh, M. R. Krishnamurthy, Mixed convective flow of Casson nanofluid in the microchannel with the effect of couple stresses: Irreversibility analysis, *Int. J. Model. Simul.*, **44** (2024), 91–105. http://dx.doi.org/10.1080/02286203.2022.2156974

37. A. Rathi, D. K. Sahoo, B. V. R. Kumar, Variational multiscale stabilized finite element analysis of transient MHD Stokes equations with application to multiply driven cavity flow, *Appl. Numer. Math.*, **198** (2024), 43–74. http://dx.doi.org/10.1016/j.apnum.2023.12.007

38. X. Li, T. Xie, Q. Wang, Z. Zhang, C. Hou, W. Guo, et al., Numerical study of the wave dissipation performance of two plate-type open breakwaters based on the Navier-Stokes equations, *J. Braz. Soc. Mech. Sci.*, **43** (2021), 1–18. http://dx.doi.org/10.1007/s40430-021-02889-7

39. X. Zhou, Z. Meng, X. Fan, Z. Luo, Analysis of two low-order equal-order finite element pairs for Stokes equations over quadrilaterals, *J. Comput. Appl. Math.*, **364** (2020), 1–12. http://dx.doi.org/10.1016/j.cam.2019.06.039

40. S. K. Das, Extension of the boundary integral method for different boundary conditions in steady-state Stokes flows, *Int. J. Numer. Meth. Fl.*, **33** (2023), 1–13. http://dx.doi.org/10.1108/hff-02-2022-0088

41. D. K. Jules, G. Hagos, K. Jonas, S. Toni, Discontinuous Galerkin methods for Stokes equations under power law slip boundary condition: A priori analysis, *Calcolo*, **61** (2024), 13. http://dx.doi.org/10.1007/s10092-023-00563-z

42. G. R. Barrenechea, M. Bosy, V. Dolean, F. Nataf, P. H. Tournier, Hybrid discontinuous Galerkin discretisation and domain decomposition preconditioners for the Stokes problem, *Comput. Method. Appl. Math.*, **19** (2019), 703–722. http://dx.doi.org/10.1515/cmam-2018-0005

43. V. Ervin, M. Kubacki, W. Layton, M. Moraiti, Z. Si, C. Trenchea, Partitioned penalty methods for the transport equation in the evolutionary Stokes-Darcy-transport problem, *Numer. Meth. Part. D. E.*, **35** (2019), 349–374. http://dx.doi.org/10.1002/num.22303

44. O. A. Ladyzhenskaya, R. A. Silverman, J. T. Schwartz, J. E. Romain, *The mathematical theory of viscous incompressible flow*, AIP, 1964. https://doi.org/10.2307/3613759

45. C. Susanne, L. Brenner, L. R. Scott, *The mathematical theory of finite element methods*, Springer, 2008. https://doi.org/10.1016/s0898-1221

46. P. Moczo, J. Kristek, M. Gális, *The finite-difference modelling of earthquake motions: Waves and ruptures*, Cambridge University Press, 2014. https://doi.org/10.1017/CBO9781139236911

47. H. Igel, *Computational seismology: A practical introduction*, Oxford University Press, 2017. https://doi.org/10.1007/s10950-017-9662-4

48. F. Brezzi, M. Fortin, *Mixed and hybrid finite element methods*, Springer-Verlag, 1991. http://dx.doi.org/10.1007/978-1-4612-3172-1

AIMS Press